CARBON letters

Original Articles
Carbon Letters Vol. 26, 11-17 (2018)

X-ray diffraction analysis of the effect of ball milling time on crystallinity of milled polyacrylonitrile-based carbon fiber

Sang-Hye Lee, Dong-Su Kang, Sang-Min Lee, and Jae-Seung Roh*

School of Materials Science and Engineering, Kumoh National Institute of Technology, Gumi 39177, Korea

Article Info

Received 15 November 2017
Accepted 19 January 2018

***Corresponding Author**
E-mail: jsroh@kumoh.ac.kr

Open Access

DOI: http://dx.doi.org/10.5714/CL.2018.26.011

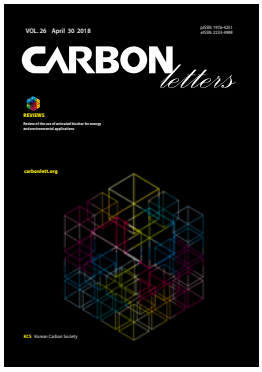

http://carbonlett.org

pISSN: 1976-4251
eISSN: 2233-4998

Abstract

Milled carbon fiber (mCF) was prepared by a ball milling process, and X-ray diffraction (XRD) diffractograms were obtained by a 2θ continuous scanning analysis to study mCF crystallinity as a function of milling time. The raw material for the mCF was polyacrylonitrile-based carbon fiber (T700). As the milling time increased, the mean particle size of the mCF consistently decreased, reaching 1.826 μm at a milling time of 18 h. The XRD analysis showed that, as the milling time increased, the fraction of the crystalline carbon decreased, while the fraction of the amorphous carbon increased. The (002) peak became asymmetric before and after milling as the left side of the peak showed an increasingly gentle slope. For analysis, the asymmetric (002) peak was deconvoluted into two peaks, less-developed crystalline carbon (LDCC) and more-developed crystalline carbon. In both peaks, Lc decreased and d_{002} increased, but no significant change was observed after 6 h of milling time. In addition, the fraction of LDCC increased. As the milling continued, the mCF became more amorphous, possibly due to damage to the crystal lattices by the milling.

Key words: ball mill, crystallinity, milled carbon fiber, PAN-based carbon fiber, X-ray diffraction, electrical conductivity

1. Introduction

Milled carbon fiber (mCF) refers to carbon fibers that are shorter than chopped carbon fibers, with a length of less than 1 mm [1]. Currently, mCF, which is usually prepared with polyacrylonitrile (PAN)-based carbon fiber or mesophase pitch-based carbon fiber, is used in various fields [2,3].

Milled PAN-based carbon fibers (mPCFs) have recently been used to improve the formability of polymer composites and to give an advantage to manufacturing. The mPCFs are also used as a filler material for functional composites to improve the conductivity of the composites [1,4-9]. Milled mesophase pitch-based carbon fibers (mMPCFs) have been studied for application as an anode material in lithium-ion batteries through graphitization heat treatment [10,11].

mPCFs are usually prepared by milling of recycled carbon fibers or by recycling of a polymer composite through combustion in a thermal degradation process [1]. The mMPCFs are prepared by a melt-blown method, ball milling, or mechanical grinding [8,9].

mMPCFs are drawing considerable attention as an anode material for batteries because they are highly anisotropic to electric and magnetic signals. The amount of lithium ions that may be included in mMPCFs, which determines the battery properties, is dependent on the crystallinity of the mMPCFs (d_{002}, Lc, La). Many researchers have reported on crystallinity in the manufacturing process, such as the mMPCF thermal treatment conditions, and the potential applicability of mMPCFs as anode materials [2,10-12].

mPCFs have recently been studied as a filler for functional composites to improve their conductivity [4-9]. Previous studies have focused on electrical conductivity as a function of the length and content of mPCFs [4-9], but few studies have been conducted on their crys-

tallinity, which is an important factor with regard to electrical conductivity.

In this study, mPCFs were prepared by ball milling of PAN-based carbon fiber, and variation in their crystallinity as a function of milling time was investigated. This article presents the variation of crystallinity analyzed by X-ray diffraction (XRD).

2. Experimental

2.1. Sample preparations

The raw carbon fiber that was used in this study was PAN-based carbon fiber T700 (12K, Toray, Japan). The raw carbon fiber was put into a tube furnace in a nitrogen atmosphere and kept at 500°C for 1 h to remove the sizing materials. The ball milling process of this study was carried out with the desized carbon fiber.

2.2. Ball milling and characterizations

The desized carbon fiber was cut to a size of 20 mm, and milled at 300 rpm using alumina balls (99.94%). The milling time was 6, 12, and 18 h. Some of the fibers were not milled by this process but formed fiber balls, which were hardened and decreased the milling efficiency. Therefore, the mCF used in this study was a fine fiber powder sorted after milling by screening classification using a 230-mesh (under 63 μm). The yield rate was defined as the ratio of the weight of the fine powder that passed through the 230-mesh to the weight of the initial fibers. Table 1 shows the yield rate of the powder as a function of milling time. Table 1 indicates that the yield rate of the powder increased as the milling time increased.

The particle size as a function of the milling time was measured using a particle-size analyzer (Master Sizer 2000, Malvern Instrument, UK). The size distribution and shape of the particle surface as well as the cross-section of the raw fiber and milled fiber were observed by scanning electron microscopy (SEM; JSM-6500F, JEOL, Japan).

2.3. XRD analysis

The variation in crystallinity as a function of milling time was analyzed by XRD (D-MAX/2500-PC, Rigaku, Japan). The wavelength of the X-ray target (Cu–Kα_1) used for the XRD was 1.5406 Å. The XRD diffractograms were obtained in the scanning range of 10° to 60° and at a scan speed of 1°/min by 2θ continuous scanning [13].

An XRD analysis was conducted by placing 0.10±0.01 g of mPCFs on the specimen holder. Measurements were conducted three times, and an annealed standard silicon sample was used to revise the 2θ position and the full-width at half-maximum (FWHM) [14].

Lu *et al*. [15] found that amorphous carbon does not contribute to the peak intensity in the XRD analysis and appears in the background. They performed a quantitative analysis by expressing the (002) peak intensity as the sum of crystalline and amorphous carbon.

The relative amounts of crystalline and amorphous carbon included in the samples before and after the milling were calculated by the maximum intensity of the (002) peak in the original XRD diffractogram before removal of the background. Fig. 1a shows the calculation method [15-18].

There have been various research results that analyzed the

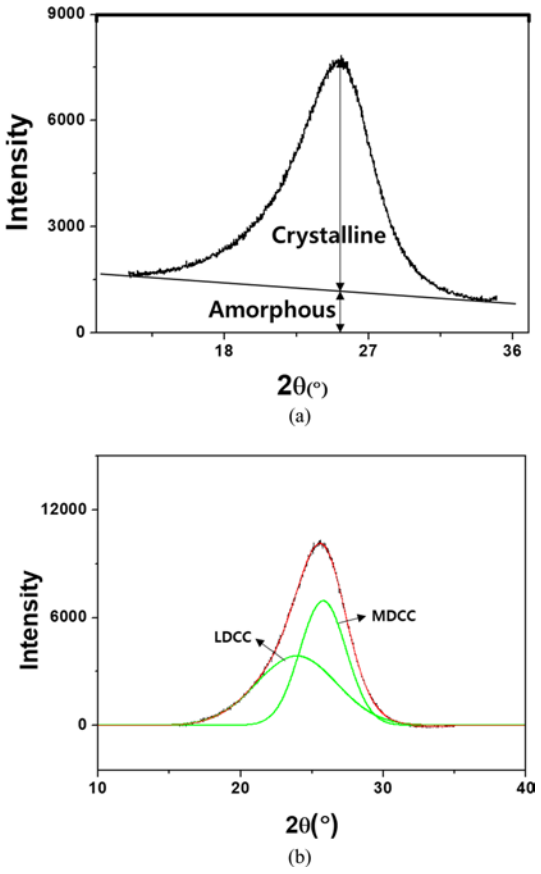

Fig. 1. (002) Peak deconvolutions of mPCFs. (a) Crystalline carbon and amorphous carbon, (b) LDCC and MDCC.

Table 1. Powder yield rate with milling time

Milling time (h)	Before milling	After milling		Yield rate (%)
	Weight of fiber (g)	Powder weight (g)	Fiber ball weight (g)	
6	5.0082	3.0084	1.0910	60.07
12	5.0105	3.5755	0.5171	71.36
18	5.0147	4.2194	-	84.14

structure parameters (d_{002}, Lc, etc.) through broad (002) peak analysis of the X-ray diffractogram. Franklin reported that non-graphitizing carbons heat treated at 3000°C showed two or three graphitization phases [19]. Addressing this result, Honda *et al*. [20] and Kobayashi *et al*. [21] deconvoluted the (002) peak into sharp peaks of 26° and 26.5° and the broad peak of 26° for the XRD analysis of phenol graphitized at a temperature range from 2,400°C to 3,000°C to calculate the d_{002} and Lc values for each peak. The d_{002} and Lc values for the broad peak of 26° were 3.42–3.45 Å and 20–40 Å, respectively. For the sharp peaks of 26° and 26.5°, the d_{002} values were 3.43–3.44 Å and 3.36 Å, respectively, and the Lc values were on the order of a few hundred Å.

Lu *et al*. [15] and Manoj *et al*. [22] proposed a deconvolution method for the (002) peak for an XRD analysis of coal. The asymmetric (002) peak deconvoluted into a γ-band of about 20° and an H-band of about 26°, and each band was defined by the number of aromatic carbon and aliphatic carbon atoms. The interlayer spacing and Lc were calculated using the 2θ and FWHM for an H-band of about 26° after (002) peak deconvolution. As the elemental carbon content increased, a decreasing tendency for d_{002} and an increasing tendency for Lc were observed.

Aladekomo *et al*. [23] and Shen *et al*. [24] proposed a deconvolution method for the (002) peak after ball milling of graphite. When $3.375 \leq d_{002} \leq 3.55$ Å, the XRD pattern was asymmetric, while $3.354 \leq d_{002} \leq 3.375$ Å of graphite had a single phase with a symmetric peak. The asymmetric peak was interpreted as a mixed phase of ordered graphite crystals of 3.34 Å and larger interlayer spacing crystals with lattice damage.

As outlined above, several researchers have analyzed crystallinity by deconvoluting the (002) peak of coal, amorphous carbon, natural graphite, and others, but reports on PAN carbon fiber are lacking.

To calculate d_{002} and Lc from the (002) peak, the base point found between 10° and 15° was connected to the region around 35° with a straight line to remove the background from the spectrucm profile.

All the (002) peaks without the background showed asymmetry. According to the XRD theory, peak asymmetry is found in samples that have a defective layer lattice structure [25]. Therefore, we assumed that the raw fiber and the milled fiber used in this study included a carbon nanocluster with fewer crystal defects and a carbon nanocluster with more crystal defects in the crystal region contributing to the (002) peak. The relative fractions of the crystal defects may be caused by the mechanical stress generated by the balls during milling. Therefore, in this study, the two carbon nanoclusters were defined as less-developed crystalline carbon (LDCC) and more-developed crystalline carbon (MDCC) relatively. After smoothing, the (002) peak without the background was deconvoluted into two bands (LDCC and MDCC) by Gaussian fitting. Fig. 1b shows the deconvolution method. The correlation coefficient of the band deconvolution was over 0.99 in all cases. The 2θ value and FWHM were obtained from each band, and the relative amounts of LDCC and MDCC were calculated from the area fractions of the bands.

The 10/peak found around 43° was analyzed by the following method. After removal of the background in the range from 35° to 60°, the (004) peak at around 52° was removed by Gaussian fitting, and then the 2θ value and the FWHM were calculated.

The interlayer spacing was calculated using Bragg's law with 2θ and FWHM values, which were obtained from each band, and the Lc and La values were calculated by Scherrer's equation.

2.4. Electrical conductivity measurement

To measure the electrical conductivity of mPCFs as a function of milling time, a powder resistivity measurement system (Han Tech Co. Ltd., Korea) was used. After the powder was poured into a 20-mm diameter mold, a 4-point probe was used to obtain the specific resistivity, which was then converted to electrical conductivity. The specific resistivity was measured by varying the pressure applied to the powder from 1.29 to 51.6 MPa.

3. Results and Discussion

3.1. Scanning electron microscopy

Fig. 2 and Table 2 show the results of the particle-size analysis. As the milling time increased, the mean particle size of the mCF decreased, reaching 1.826 μm at a milling time of 18 h. As seen in Fig. 2, the particle-size distribution was bi-modal rather than a normal distribution. This may be because the milling was a non-uniform process in which the fibers, the starting raw material, gradually changed to granular particles. The non-uniformity of the milling process was confirmed by SEM.

Fig. 3 shows 500-magnification SEM images of the particle distribution as a function of the milling time of the T700 fiber. The fibers gradually changed to fine particles as the milling time

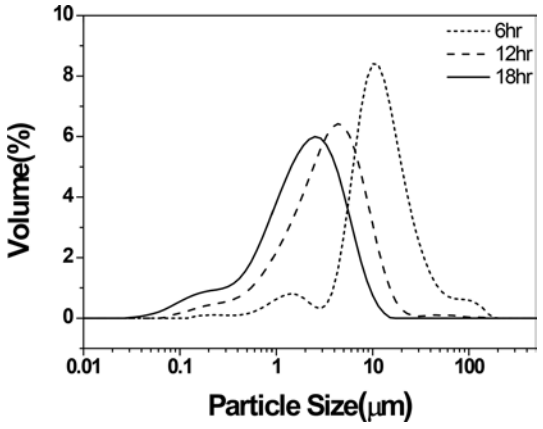

Fig. 2. Particle size changes as a function of milling time.

Table 2. Particle size changes as a function of milling time

Milling time (h)	D_{10} (μm)	D_{50} (μm)	D_{90} (μm)
6	4.177	10.632	29.394
12	0.753	3.246	8.634
18	0.346	1.826	5.084

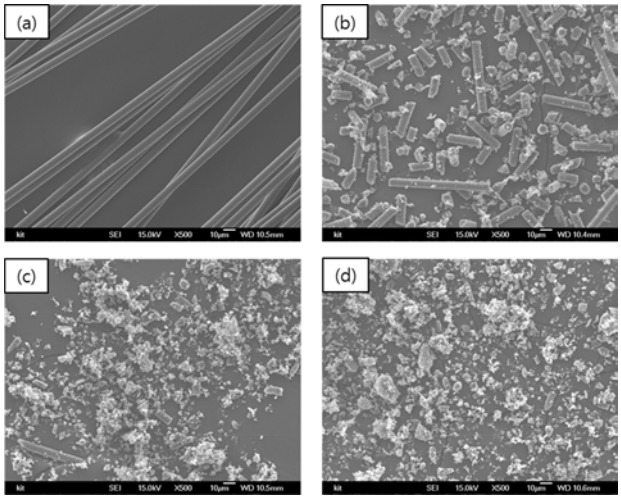

Fig. 3. SEM images of mPCFs (X500) (a) desized mPCFs, (b) 6 h, (c) 12 h, and (d) 18 h.

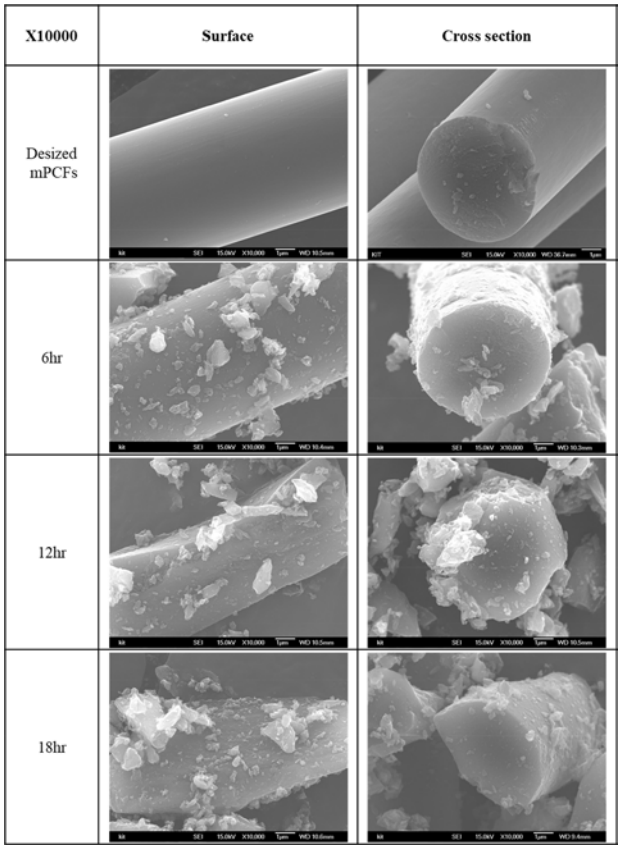

Fig. 4. SEM images of surface and cross section of mPCFs (×10,000).

increased. After 18 h of milling, fibrous particles with a length of over 10 μm were rare, as most of the fibers changed to fine particles.

Fig. 4 is 10,000-magnification SEM images showing the surface and the cross-section of the milled fiber. The magnified images show that the fibers were not uniformly milled by ball milling. Fig. 4 shows that the some of the fibers were broken in the length direction (decrease of the diameter) and others were attached to a large particle and maintained the shape of a fiber. The milling process was likely non-uniform because the carbon fiber was anisotropic and had a non-uniform cross-sectional microstructure [26]. Due to the non-uniform microstructure, it is difficult to obtain fine spherical particles by milling.

3.2. XRD analysis

Fig. 5 shows the XRD diffractograms as a fucntion of milling time. The XRD analysis showed that as the milling time increased, I_{002} decreased but I_{10l} increased. As seen in the previous SEM images, as the milling time increased, the fibers became smaller particles that could be arranged more randomly in the XRD sample holder. As a result, the cross-section of the fibers was exposed to the incident X-ray beam; thus, the diffraction peak of I_{10l} could be more easily obtained.

In addition, the (100) and (101) peaks were not completely deconvoluted from the (10*l*) peak, which indicates that mPCFs may have a turbostratic structure and include many defects inside the fiber [27].

Table 3 and Fig. 6 show the variation in the structural parameters of the raw material fiber and the mPCFs as a fuction of milling time. For the raw material fiber, the d_{002} and Lc values were 3.7 Å and 14.2 Å, respectively, in the LDCC band, and 3.45 Å and 24.71 Å, respectivley, in the MDCC band, indicating that the MDCC was more crystalline. The d_{002} value of the LDCC and MDCC slightly increased after 6 h of milling, but the d_{002} value underwent few changes as the milling time increased

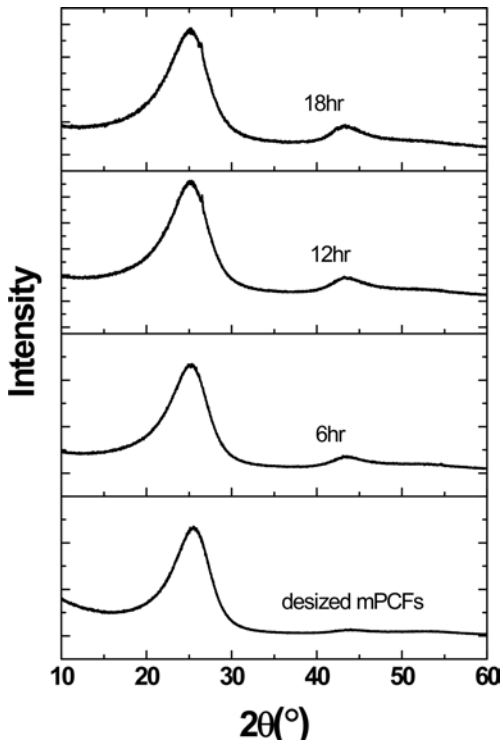

Fig. 5. XRD diffractograms of mPCFs as a function of milling time.

Table 3. Structural parameters of the mPCFs

Milling time (h)	002 Peak (LDCC)				002 Peak (MDCC)				10*l* Peak			
	2θ	d_{002} (Å)	FWHM	Lc (Å)	2θ	d_{002} (Å)	FWHM	Lc (Å)	2θ	d10l (Å)	FWHM	La (Å)
0	23.91	3.719	5.649	14.2	25.78	3.453	3.261	24.7	44.24	2.046	3.532	49.6
	23.70	3.751	6.359	12.6	25.62	3.474	3.370	23.9	44.16	2.049	3.379	51.9
	23.52	3.780	6.985	11.5	25.64	3.472	3.299	24.4	44.29	2.043	3.283	53.4
6	23.38	3.802	6.811	11.8	25.38	3.507	3.424	23.5	43.65	2.072	3.451	50.7
	23.45	3.791	6.901	11.6	25.43	3.500	3.372	23.9	43.61	2.074	3.425	51.1
	23.47	3.787	7.080	11.3	25.55	3.483	3.419	23.6	43.77	2.067	3.530	49.6
12	23.32	3.811	7.193	11.2	25.35	3.511	3.514	23.0	43.57	2.076	3.562	49.1
	23.48	3.785	6.741	11.9	25.40	3.503	3.381	23.4	43.59	2.074	3.435	50.9
	23.47	3.788	7.278	11.0	25.62	3.475	3.423	23.5	43.86	2.063	3.446	50.8
18	23.34	3.808	7.141	11.2	25.33	3.513	3.502	23.0	43.47	2.080	3.372	51.9
	23.31	3.813	6.986	11.5	25.38	3.506	3.383	23.8	43.47	2.080	3.264	53.6
	23.45	3.790	7.096	11.3	25.49	3.491	3.420	23.6	43.55	2.077	3.326	52.6

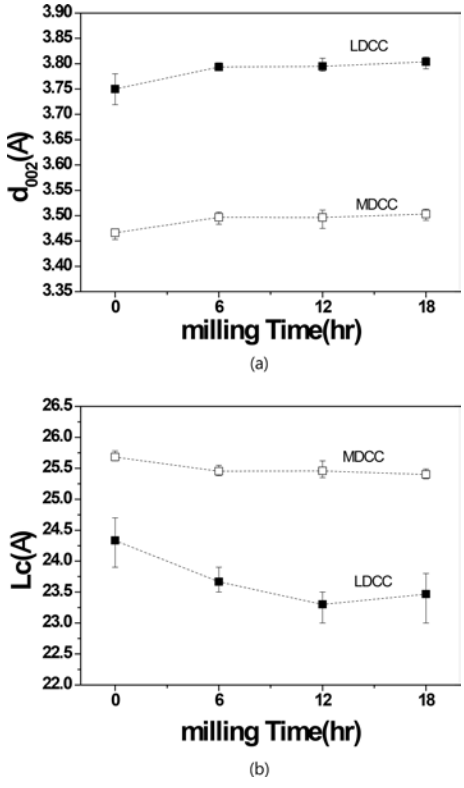

Fig. 6. Structural parameter changes of the mPCFs (a) d_{002} and (b) Lc.

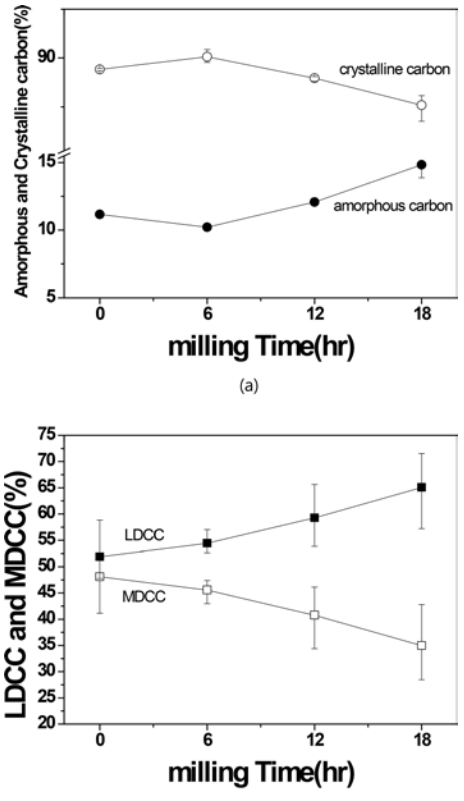

Fig. 7. Crystalline changes of mPCFs with milling time. (a) Fractions of amorphous carbon and crystalline carbon and (b) fractions of LDCC and MDCC.

further. The Lc value of the MDCC slightly decreased after 6 h of milling, but it showed little decrease as the milling time increased further. As a result of the structural parameters, both the d_{002} and Lc values showed considerable change at 6 h of milling and had few changes as the milling time increased further. We considered that the changes in crystallinity occurred most during the initial milling process.

Fig. 7a shows the variation of the relative fractions of crystsalline carbon and amorphous carbon. In the initial raw material fiber, the fractions of crystalline carbon and amorphous carbon were 88.7% and 11.3%, respectively, indicating that the fraction of the crystalline carbon was much higher. As the milling time increased, the fraction of amorphous carbon increased continuously to 14.2% after 18 h of milling, which was 2.9% higher than that of the initial raw material fibers. The fraction of crystalline carbon showed the opposite tendency. Therefore, as the

milling continued, the crystals of the fiber samples seem to have become more amorphous.

Fig. 7b shows the relative LDCC and MDCC fractions as a fuction of milling time. In the initial raw material fiber, the LDCC fraction was 49.1%, and the MDCC fraction was 50.88%. As the milling time increased, the fraction of the LDCC increased continuously to 57.2% after 18 h of milling, which was 8.09% higher than that of the initial raw material fibers. The MDCC fraction showed the opposite tendency. Therefore, as the amount of LDCC increased with milling time, the crystals of the samples seem to have gradually become amorphous.

Shen *et al*. [24] prepared a nanocrystalline graphite mixed with an amorphous phase by increasing the time for milling graphite flakes. As the milling time increased, the (002) peak became asymmetric. This was explained by the presence of a relatively well arranged graphite with an interlayer spacing of 0.340 nm and a graphite with damaged lattices with a larger interlayer spacing. As the milling time increased, a graphite powder could be prepared as a mixture of nanocrystalline graphite and amorphous graphite. The amorphization caused by the milling was explained as an instaneous high-pressure effect, which we considered a valid intepretation of the results. Hence, the method of analyzing the crystallinity of mPCFs through the deconvolution of an asymmetric diffraction peak was validated as a very useful analysis method.

3.3. Electrical conductivity measurement

Fig. 8 shows the conductivity and mean particle-size variation as a function of the amorphous carbon fraction of mPCFs. The conductivity was measured when the pressure was 51.6 MPa, which fell in the range of 1.29 to 51.6 MPa where the specific resistivity was most stable. The fraction of amorphous carbon increased with milling time, and the conductivity and mean particle size of the mPCFs showed decreasing tendencies. These results seem to be due to a defect factor that impeded the movement of electrons as the lattice defect region (amorphous region) relatively increased. Therefore, when milling was carried out for an extended time, the amorphous carbon region increased due to the defect region from the lattice damage and amorphization, which had a negative impact on the electrical conductivity. Thus, a milling time of 6 h was determined to be the ideal condition for fabricating a conductive composite material.

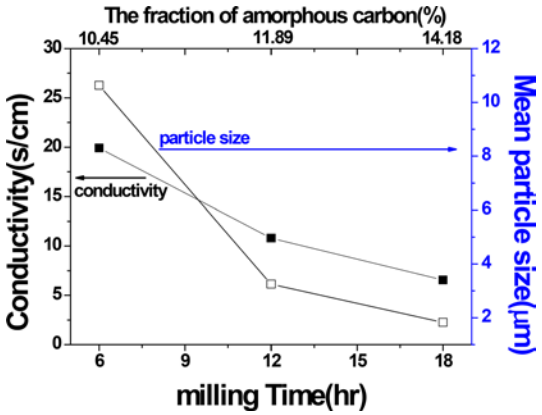

Fig. 8. Conductivity and mean particle-size changes of mPCFs with milling time.

4. Conclusions

In this study, a PAN-based carbon fiber, T700 fiber, was milled by ball milling, and the variation in its crystallinity was analyzed by XRD. We made the following conclusions based on the experimental results.

The raw material fiber changed to fine particles as the milling time increased, but the fine particles prepared by milling were non-uniform. The milling was non-uniform likely because the carbon fiber was anisotropic and had a non-uniform cross-sectional microstructure.

The structural parameters of the raw material fiber and the mPCFs were calculated by decomposing the (002) peak. As the milling time increased, the d_{002} value increased and the Lc value decreased. As a result of the structural parameters, both the d_{002} and Lc values showed considerable change at 6 h of milling and showed few changes as the milling time increased further. We concluded that the changes in crystallinity occurred most during the initial milling process.

We observed the variation in the fractions of crystalline carbon and amorphous carbon by deconvoluting the (002) peak. As the milling time increased, the amorphous carbon fraction increased, which indicates that the crystals of the samples may have become more amorphous through continued milling.

Further, we analyzed the fractions of the LDCC and the MDCC as a function of milling time. As the milling time increased, the LDCC fraction continuously increased, indicating that the crystals of the samples may have become more amorphous as milling continued.

mPCFs were used as fillers to enhance the conductivity of the composites. As the milling time increased, the mean particle size decreased along with the electrical conductivity. We determined that this result was due to the fraction of amorphous carbon from the milling process.

Conflict of Interest

No potential conflict of interest relevant to this article was reported.

Acknowledgements

This study was financially supported by Kumoh National Institute of Technology.

References

[1] Wu C, Feng P, Bai Y, Lu Y. Epoxy enhanced by recycled milled carbon fibres in adhesively-bonded CFRP for structural strengthening. Polymers, 6, 76 (2014). https://doi.org/10.3390/polym6010076.

[2] Nishimura Y, Takahashi T, Tamaki T, Endo M, Dresselhaus MS. Anode performance of B-doped mesophase pitch-based carbon fibers in lithium ion secondary batteries. Tanso, 172, 89 (1996). https://doi.org/10.7209/tanso.1996.89.

[3] Takami N, Satoh A, Hara M, Ohsaki T. Rechargeable lithium-ion cells using graphitized mesophase-pitch-based carbon fiber anodes. J Electrochem Soc, 142, 2564 (1995). https://doi.org/10.1149/1.2050054.

[4] Thongruang W, Spontak RJ, Balik CM. Correlated electrical conductivity and mechanical property analysis of high-density polyethylene filled with graphite and carbon fiber. Polymer, 43, 2279 (2002). https://doi.org/10.1016/s0032-3861(02)00043-5.

[5] Ozkan C, Karsli NG, Aytac A, Deniz V. Short carbon fiber reinforced polycarbonate composites: Effects of different sizing materials. Compos Part B Eng, 62, 230 (2014). https://doi.org/10.1016/j.compositesb.2014.03.002.

[6] Zakaria MY, Sulong AB, Sahari J, Suherman H. Effect of the addition of milled carbon fiber as a secondary filler on the electrical conductivity of graphite/epoxy composites for electrical conductive material. Compos Part B Eng, 83, 75 (2015). https://doi.org/10.1016/j.compositesb.2015.08.034.

[7] Kasgoz A, Akın D, Durmus A. Rheological and electrical properties of carbon black and carbon fiber filled cyclic olefin copolymer composites. Compos Part B Eng, 62, 113 (2014). https://doi.org/10.1016/j.compositesb.2014.02.017.

[8] Wang C, Li KZ, Li HJ, Jiao GS, Lu J, Hou DS. Effect of carbon fiber dispersion on the mechanical properties of carbon fiber-reinforced cement-based composites. Mater Sci Eng A, 487, 52 (2008). https://doi.org/10.1016/j.msea.2007.09.073.

[9] Mathur RB, Dhakate SR, Gupta DK, Dhami TL, Aggarwal RK. Effect of different carbon fillers on the properties of graphite composite bipolar plate. J Mater Process Tech, 203, 184 (2008). https://doi.org/10.1016/j.jmatprotec.2007.10.044.

[10] Endo M, Kim C, Karaki T, Kasai T, Matthews MJ, Brown SDM, Dresselhaus MS, Tamaki T, Nishimura Y. Structural characterization of milled mesophase pitch-based carbon fibers. Carbon, 36, 1633 (1998). https://doi.org/10.1016/s0008-6223(98)00157-2.

[11] Endo M, Kim C, Karaki T, Nishimura Y, Matthews MJ, Brown SDM, Dresselhaus MS. Anode performance of a Li ion battery based on graphitized and B-doped milled mesophase pitch-based carbon fibers. Carbon, 37, 561 (1999). https://doi.org/10.1016/s0008-6223(98)00222-x.

[12] Salver-Disma F, Tarascon JM, Clinard C, Rouzaud JN. Transmission electron microscopy studies on carbon materials prepared by mechanical milling. Carbon, 37, 1941 (1999). https://doi.org/10.1016/s0008-6223(99)00059-7.

[13] Lee SM, Kang DS, Kim WS, Roh JS. Fabrication of isotropic bulk graphite using artificial graphite scrap. Carbon Lett, 15, 142 (2014). https://doi.org/10.5714/cl.2014.15.2.142.

[14] Kercher AK, Nagle DC. Microstructural evolution during charcoal carbonization by X-ray diffraction analysis. Carbon, 41, 15 (2003). https://doi.org/10.1016/s0008-6223(02)00261-0.

[15] Lu L, Sahajwalla V, Kong C, Harris D. Quantitative X-ray diffraction analysis and its application to various coals. Carbon, 39, 1821 (2001). https://doi.org/10.1016/s0008-6223(00)00318-3.

[16] Franklin RE. The interpretation of diffuse X-ray diagrams of carbon. Acta Crystallogr, 3, 107 (1950). https://doi.org/10.1107/s0365110x50000264.

[17] Ergun S, Tiensuu VH. Interpretation of the intensities of X-rays scattered by coals. Fuel, 38, 64 (1959).

[18] Roh JS. Microstructural changes during activation process of isotopic carbon fibers using CO_2 Gas(I)-XRD study. Korean J Mater Res, 13, 742 (2003). https://doi.org/10.3740/MRSK.2003.13.11.742.

[19] Franklin RE. Crystallite growth in graphitizing and non-graphitizing carbons. Proc R Soc A Math Phys Eng Sci, 209, 196 (1951). https://doi.org/10.1098/rspa.1951.0197.

[20] Honda H, Kobayashi K, Sugawara S. X-ray characteristics of non-graphitizing-type carbon. Carbon, 6, 517 (1968). https://doi.org/10.1016/0008-6223(68)90091-2.

[21] Kobayashi K, Sugawara S, Toyoda S, Honda H. An X-ray diffraction study of phenol-formaldehyde resin carbons. Carbon, 6, 359 (1968). https://doi.org/10.1016/0008-6223(68)90030-4.

[22] Manoj B, Kunjomana AG. Study of stacking structure of amorphous carbon by X-ray diffraction technique. Int J Electrochem Sci, 7, 3127 (2012).

[23] Aladekomo JB, Bragg RH. Structural transformations induced in graphite by grinding: Analysis of 002 X-ray diffraction line profiles. Carbon, 28, 897 (1990). https://doi.org/10.1016/0008-6223(90)90338-y.

[24] Shen TD, Ge WQ, Wang KY, Quan MX, Wang JT, Wei WD, Koch CC. Structural disorder and phase transformation in graphite produced by ball milling. Nanostruct Mater, 7, 393 (1996). https://doi.org/10.1016/0965-9773(96)00010-4.

[25] Schossberger F. Advances in X-ray Analysis, 1st ed., Plenum Press, New York, 73 (1957).

[26] Oh SM, Lee SM, Kang DS, Roh JS. Microstructural changes of polyacrylonitrile-based carbon fibers (T300 and T700) due to isothermal oxidation (1): focusing on morphological changes using scanning electron microscopy. Carbon Lett, 18, 18 (2016). https://doi.org/10.5714/cl.2016.18.018.

[27] Roh JS. Structural changes during oxidation process of anisotopic mesophase carbon fibers(I): TEM and XRD study. Korean J Mater Res, 13, 825 (2003). https://doi.org/10.3740/mrsk.2003.13.12.825.